Polymer 51 (2010) 5756–5763

Contents lists available at ScienceDirect

Polymer

journal homepage: www.elsevier.com/locate/polymer

Processing dependence of surface morphology in condensation cured PDMS nanocomposites

Souvik Chakrabarty [a], Xiaojuan Zhang [a], Puja Bharti [a], Yoshiki Chujo [b], Junpei Miyake [b], Kenneth J. Wynne [a,*], Vamsi K. Yadavalli [a,**]

[a] Chemical and Life Science Engineering Department, School of Engineering, Virginia Commonwealth University, 601 West Main Street, Richmond, VA 23284-3028, USA
[b] Department of Polymer Chemistry, Graduate School of Engineering, Kyoto University, Katsura, Nishikyo-ku, Kyoto 615-8510, Japan

ARTICLE INFO

Article history:
Received 12 July 2010
Received in revised form
17 September 2010
Accepted 21 September 2010
Available online 1 October 2010

Keywords:
PDMS
PDES
High speed mixing

ABSTRACT

A processing method using high speed mixing was developed for the generation of nanocomposites comprised of α,ω-dihydroxy-polydimethylsiloxane (PDMS) and untreated fumed silica nanoparticles (U-FSN). Conventional condensation cure with poly(diethoxysiloxane) (PDES) was employed so as to generate PDMS/FSN nanocomposites with increasing weight fractions of siliceous domain. This study focuses on the changes in surface morphology imaged by non-contact or tapping mode AFM (TM-AFM) as a function of increasing the initial concentration of PDES. The ratios (X) of Si–OEt from PDES to Si–OH from PDMS end groups are 4X, 14X, 28X, 35X, 45X and 60X. Compared to prior work, two important differences in the present investigation are (1) the use of a high shear mixer as a processing tool to facilitate nanoparticle dispersion and (2) spin coating instead of dip coating. Common to the present and prior work is the use of TM-AFM for investigating surface morphology as a function of siliceous phase precursor concentration. TM-AFM phase images show nanoparticles are "reporters" and reflect effects of composition and processing on surface morphology. Near-surface nanoparticles are clearly imaged up to 35X, "disappear" at 45X, then "reappear" at 60X. These results are different from those previously reported where "disappearance" was noted for 14X compositions. The differing results reveal that processing conditions have an important effect on surface morphology. A model is presented that accounts for the surface morphological observations and wetting behavior via sessile drop measurements.

1. Introduction

Research in hybrid nanocomposites seeks optimization of performance by combining synergistically organic and inorganic materials [1–9]. Nanoparticle interfacial modification is an essential part of engineering optimal compositions. This is demonstrated by the discovery of dramatic improvements in mechanical properties for clay polymer nanocomposites [10] which resulted in a new materials research field that is still of great interest [11,12]. Expanding studies in nanocomposites seek to improve performance in diverse areas such as dielectrics [13] and hybrid photovoltaics [14].

Silicone elastomers have weak mechanical properties [15–17] and require fillers to provide reinforcement. As a result, one of the most common hybrid nanocomposites, which has been known for decades [18] is comprised of a polydimethylsiloxane matrix combined with fumed silica nanoparticles (FSN) [19–22]. In addition to fumed silica nanoparticles, zeolite [23] ceramic [24] and silica nanoparticles [25,26] have been utilized.

Polydimethylsiloxane elastomers have very low glass transition temperatures (T_g ~ −120 °C) and high thermal stability (~250 °C) [27]. Hydrophobicity, easy fabrication and biocompatibility [28,29], have led to a wide range of applications including caulks, adhesives and coatings [30] biomaterials [31] and even in tissue engineering [32].

We have explored surface science associated with several sol–gel cured PDMS systems. To improve oleophobicity, hydroxyl-terminated polydimethysiloxane, PDMS(OH)$_2$, was crosslinked with (tridecafluoro-1,1,2, 2-tetrahydrooctyl)triethoxysilane (FTEOS). The surface morphology depended strongly on the PDMS/crosslinker ratio [33]. For example, at a ratio of 6X (X = Si–OEt/Si–OH), micron scale, fluorous siliceous domains were observed surrounded by siloxane rich domains [33]. In contrast, at a ratio of 12X, a uniform surface layer of the fluorous siliceous phase formed, which was confirmed by XPS and high advancing contact angles. Although the goal of oleophobicity was attained, the fluorous siliceous domain is brittle, limiting applications [34].

* Corresponding author. Tel.: +1 804 828 9303; fax: +804 828 3846.
** Corresponding author. Tel.: +1 804 828 0587; fax: +804 828 3846.
E-mail addresses: kjwynne@vcu.edu (Kenneth J. Wynne), vyadavalli@vcu.edu (V. K. Yadavalli).

0032-3861/$ – see front matter © 2010 Elsevier Ltd. All rights reserved.
doi:10.1016/j.polymer.2010.09.053

PDES is poly(diethoxysiloxane), with the approximate empirical formula $[SiO(CH_3CH_2O)_2]_n$ or $[SiO(OEt)_2]_n$. While tetraethylorthosilicate (TEOS) volatilizes during hydrolysis and condensation cure of $PDMS(OH)_2$, low volatility and relatively low condensate (ethanol) generation make PDES very useful alternative [35,36]. A time dependent surface morphology and stability was found for PDMS/PDES coatings [33].

PDES and related condensation cure agents are typically used at ~5 wt% or less. Such low sol–gel curing agent content minimizes shrinkage and generation of volatiles from condensation cure. To explore the impact of increasing siliceous domain content, the surface and bulk morphology of elastomeric coatings comprised of $PDMS(OH)_2$, fumed silica nanoparticles and increasing PDES content (Scheme 1) was investigated by tapping mode atomic force microscopy (TM-AFM) [37,38]. It is important to note that mixing was performed manually at ambient temperature; herein, this process is designated very low speed (VLS) mixing. For U-FSN (14 wt %) and complete cure at 100 °C, the bulk nanoparticle/PDMS matrix morphology was conventional. Unexpectedly, near-surface nanoparticles acted as morphological "reporters", revealing a surface morphology dependent on the mole ratio of OEt_{PDES}/OH_{PDMS} designated by "X": (1) 5X, nanoparticles imaged, "expected"; (2) 14X, nanoparticles "disappear"; (3) 28X, nanoparticles "reappear".

Water is both a reactant (–Si–O–Et hydrolysis) and product (Si–OH condensation) in alkoxysiloxane cure using $[SiO(OEt)_2]_n$. Therefore, in addition to crosslinking HO(PDMS)OH, a glassy siliceous domain is formed. The "appearing" and "disappearing" nanoparticle phenomenon noted above was explained by a model that related the AFM tip interaction with the increasing near-surface siliceous domain content and nanoparticle surface chemistry. With very low speed (VLS) processing conditions used previously, increasing PDES content to 14X resulted in a near-surface siliceous layer that isolated the AFM tip from near-surface untreated fumed silica nanoparticles (U-FSN, disappearing, Fig. 7B). Increasing the siliceous content further (28X) resulted in a near-surface siliceous volume fraction high enough to encompass the near-surface nanoparticles and facilitate mechanical detection by the tip (reappearing). The analogy that was employed to explain this unexpected phenomenon was as follows: when blindfolded, it is easy to detect a slightly submerged rock under water; however, it is not possible to detect the rock if a thin layer of ice intervenes. If the ice becomes thick enough to contact the rock, it is possible to locate the rock due to a lower sound when tapping.

VLS mixing employed in the above study is tedious and the extent of nanoparticle dispersion is "operator dependent". On a large scale, mixing viscous silicone macromonomers with fillers is done via extruders or other mechanical devices so as to obtain uniform filler dispersion. To mimic such processes a small scale device for high speed (HS) mechanical mixing was used for the nanocomposite processing reported herein. Processing the same PDMS nanocomposite compositions via HS mixing provides near-surface morphologies that are surprisingly different compared to VLS mixing. While the same morphological sequence (appearing, disappearing, reappearing) is "reported" by near-surface nanoparticles, different compositions for these events are observed and the changes imaged by TM-AFM are more subtle. In view of the importance of understanding nanocomposite morphology and nanoparticle interfaces and their relationships to the synergistic development of hybrid materials properties, these results are presented herein.

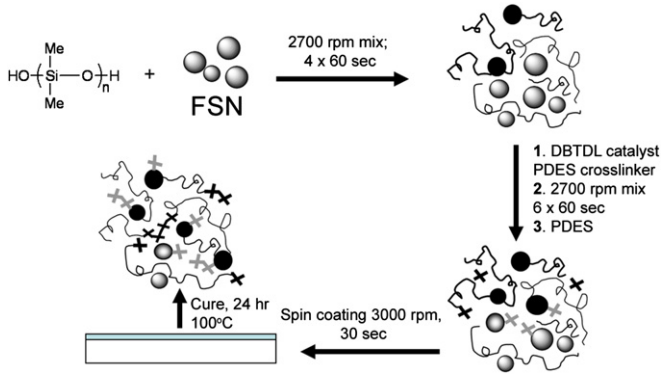

Scheme 1. Processing sequence for PDMS-FSN nanocomposites. The filled circles represent nanoparticles to which –Si–OH chain ends are bound. A grey x indicates covalent bonding of $-Si(-O-)_3$ to FSN.

2. Experimental

2.1. Materials

Silanol terminated polydimethylsiloxane (DMS-S31, 1000 cSt, 26 kDa) was obtained from Gelest Inc. Unmodified fumed silica nanoparticles (U-FSN, Aerosil 300 fumed silica unmodified) having a diameter of 50 nm and a surface area of 300 ± 30 sqm/g was obtained from Aerosil. Modified fumed silica nanoparticles (T-FSN, Cab-o-sil TS530 HMDZ treated fumed silica) having a BET surface area of 200 sqm/g was generously provided by Quantum Silicones, Midlothian, VA. Polydiethoxysiloxane (PDES) containing 40–42% SiO_2 equivalent (ES40) was obtained from Gelest; dibutyltin dilaurate (DBTDA) was obtained from Aldrich.

2.2. FSN-PDMS nanocomposite preparation and processing

Fumed silica/PDMS nanocomposite coatings were prepared in two steps. Initial nanoparticle dispersion was followed by further nanoparticle dispersion and catalyst/PDES mixing.

2.2.1. Nanoparticle dispersion

Hydroxy-terminated polydimethylsiloxane (5 g), unmodified fumed silica nanoparticles (U-FSN, 0.71 g, 14 wt%) were placed in a 50 g capacity Flacktek containers having a screw top. The container was placed in a Speed Mixer-DAC 150FV (Flacktek Inc., LandrumSC). The protocol entails the use of a 'High-Speed' (HS) mixing technique which involves mixing the ingredients in a cycle of 2700 rpm for 60 s. This HS mixing process was repeated 4 times to obtain a highly viscous, whitish nanoparticle/PDMS dispersion. The rotary motion and shear combined to increase the temperature of the nanoparticle/PDMS dispersion from ambient (25 °C) to 30 °C.

2.2.2. Catalyst/PDES mixing

The metric for defining quantities of PDES crosslinker/siliceous domain precursor is the ratio (X) of Si–O–Et groups from PDES to Si–OH groups $[PDMS(OH)_2]$. To explore a wide range of siliceous domain content, 4, 14, 28, 35, 45, and 60X compositions were obtained. Calculated amounts (Table 1) of PDES and 0.5 wt% DBTDA catalyst were added to the nanoparticle PDMS dispersion obtained as described above in step (a). The mixture was processed at 2700 rpm for 60 s, which is the maximum processing time for the machine. After a 10 s interval, this process was repeated 5 times to ensure homogeneity. The temperature of the resin mixture at this point was 40 °C. After a total of six mixing cycles the viscosity of the whitish resin was noticeably diminished by a combination of temperature and shear thinning. This decreased viscosity facilitated spin coating slides for surface analysis. Samples were spun coated on glass slides for 30 s at 3000 rpm, and cured for 72 h at 100 °C. Previous work had established that these conditions would effect complete cure [38]. Although the nanoparticle/resin mixture was

Table 1
Composition of filled U-FSN nanocomposites.

PDES, g (mmoles OEt)[a] (wt%)	Siliceous domain[c] (wt%)	Ratio "X"[b]	U-FSN, g (wt%)	Shrinkage (vol%)
0.104 (0.77) (2.1)	0.87	4	0.72 (14.2)	1.03
0.363 (2.68) (7.3)	3.1	14	0.75 (14.5)	3.44
0.72 (5.33) (14.5)	6.1	28	0.8 (15)	6.51
0.91 (6.74) (18.2)	7.6	35	0.83 (15.4)	7.9
1.17 (8.67) (23.4)	9.7	45	0.87 (15.8)	9.7
1.56 (11.55) (31.2)	13	60	0.92 (16)	12.3

[a] DBTDA catalyst (0.025 g) and mass of PDMS (5.0 g) were held constant.
[b] X = Si(OEt)/Si(OH).
[c] Calculated SiO_2 weight % (from PDES) in the nanocomposite.

whitish-translucent, spin coating resulted in the formation of thin (ca. 30 μm), homogenous, optically transparent films.

2.2.3. Preparation of fracture surfaces

The processed PDMS resin containing U-FSN was poured into Petri dishes and was allowed to cure for 72 h at 100 °C. The resulting U-FSN/PDMS nanocomposite was dipped in liquid nitrogen and fractured to obtain a smooth surface.

2.3. AFM imaging

PDMS nanocomposite morphologies were investigated using TM-AFM instruments from Asylum Research, Santa Barbara, CA (MFP-3D) and Veeco Instruments, PlainviewNY (DI-3100). For the MFP-3D, Olympus AC 240 TS cantilevers were used with a nominal spring constant in the range of 0.7 N/m–3.8 N/m. For the DI-3100 a Veeco Nanoscope V controller was utilized with Veeco RTESPW cantilevers (part: MPP-11100-W) having nominal spring constants in the range of 20 N/m–80 N/m. A scan rate of 1 Hz was used for all imaging. For comparisons, AFM images are normalized to the same phase scale (z, deg) as indicated in Figure legends. The phase scale is chosen to optimize image quality and consistency with topographical images.

Phase images provide contrast between near-surface regions of higher and lower modulus [39]. With the Nanoscope instrument, the default is light for regions of higher modulus and dark for softer regions. For example, an evolution of clearly defined surface domains was observed for condensation cured PDMS modified with a fluorous triethoxysilane [40]. Similarly, for polyurethanes, near-surface hard block domains appear light while soft block domains are dark [41–44]. Inspection of images previously reported for PDMS nanocomposites [37,38] shows that near-surface nanoparticles appear dark while the "soft" silicone matrix is light. This representation is opposite to the earlier work noted above [40].

Garcia first modeled a phase inversion phenomenon that recognized attractive and repulsive operational modes in TM-AFM [45]. In one mode, a net attractive force dominates the amplitude reduction while in the other a net repulsive force controls cantilever dynamics. Garcia's analysis showed that stiff samples give rise to large repulsive forces (a net positive force), while compliant materials give an opposite result. Changing the drive frequency, which controls tip–sample interactions can access both regimes so that the phase image representation for the same sample can be reversed [45–47].

Garcia's analysis explains why the glassy, microscale surface features formed by the fluorous modifier were light/high modulus – dark/low modulus [40] while more compliant PDMS nanocomposites have reversed appearances. In the present paper, phase images are compared that often have opposite phase image representations for the same sample, but the underlying morphological structure is, of course, identical. The contrasting images are noted as "phase image reversal" or PIR in the appropriate points in the discussion.

2.4. Wetting behavior

Static contact angles were obtained using a Rame-Hart goniometer equipped with an LCD camera. Deionized water (~18.2 MΩ) was used as the probe liquid. A water drop was placed on the coated surface and the image was taken immediately. Captured

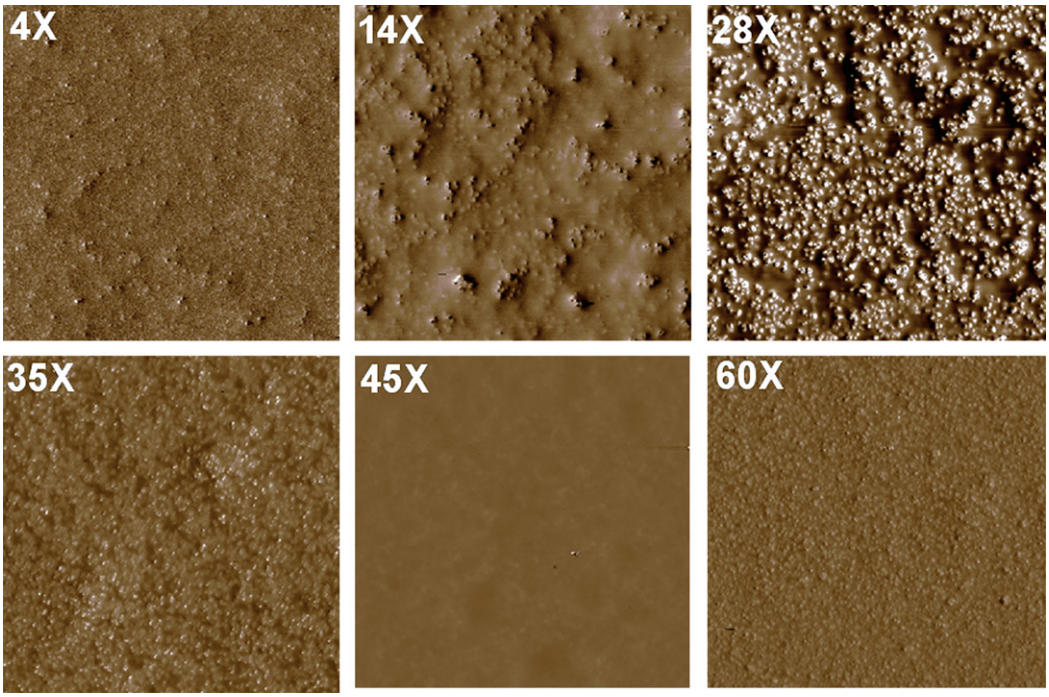

Fig. 1. Phase images (20 × 20 μm, $z = 30°$) for U-FSN-PDMS samples cured at 100 °C for 72 h.

images were analyzed and contact angles were obtained using Dropview image software version 1.4.11. Average values were obtained for 10 observations (2 drop sites, 5 readings each).

3. Results

The combination of hydroxyl-terminated PDMS, untreated fumed silica nanoparticles (U-FSN) and increasing amounts of polydiethoxysiloxane (PDES), that is, increased siliceous domain content, led to the unexpected surface phenomenon of "appearing" and "disappearing" nanoparticles [38]. This was followed by "reappearing" nanoparticles at even higher PDES concentrations [37]. These results attest to the sensitivity of TM-AFM to subtle changes in nanoscale surface morphology for condensation cured PDMS. The work reported herein emerged from an effort to simplify and improve reproducibility of mixing viscous PDMS resin/nanoparticle combinations. Considering the straightforward formulation and nominally similar processing the TM-AFM results were surprising.

3.1. Compositions

Dihydroxy-terminated PDMS (26 kDa) and FSN (14 wt%) were used to generate a series of nanocomposites. By increasing the PDES crosslinker/siliceous phase precursor, compositions with increasing siliceous domain (SD) were prepared (Table 1). In an earlier investigation, a "Very Low-Speed" (VLS) mixing technique was employed involving mixing the ingredients in a cycle of 100 rpm for 60 s. In contrast to the earlier study, compositions were processed with a high speed (HS) mixing technique described earlier to obtain finely dispersed nanoparticles.

Scheme 1 illustrates the processing sequence, which is critical to the development of surface morphologies described in the next section. First, four HS mixing cycles accomplish initial homogenization. Second, PDES and catalyst were added followed by six HS mixing cycles. During this sequence a noticeable decrease in viscosity occurred, but the bulk resin mixture remained whitish-opaque. After spin coating and cure at 100 °C, optically transparent 30 μm films were obtained.

3.2. PDMS/U-FSN surface morphology

TM-AFM phase images (20 × 20 μm, Asylum MFP-3D) are shown in Fig. 1 for U-FSN nanocomposites with increasing siliceous content ("X") but similar U-FSN weight percents. As the weight fraction of siliceous content increases (4X to 28X) near-surface nanoparticles are imaged with increasing clarity. At 35X nanoparticle imaging is subdued while nanoparticles "disappear" at 45X. At 60X nanoparticles "reappear", though the resolution is modest.

The results in Fig. 1 confirm previous results that U-FSN act as "reporters" for near-surface morphological changes [37,38]. However, the sequence of observed morphologies is completely different from those previously reported [37,38]. To confirm the unexpected results, a new set of samples were processed (Scheme 1) and imaged with a Veeco Nanoscope V system (Figure S1). The sequence of phase images in Figure S1 is essentially the same as those in Fig. 1, although the contrasting imaging colors are opposite due to phase image reversal (PIR) described in the Experimental section. Thus, convinced that the nanoparticles are "reporting" an important effect for the new processing sequence, we set about interpreting the "message".

To focus more clearly on nanoscale surface morphology, Fig. 2 shows 5 × 5 μm phase images for the same composition range imaged in Fig. 1 at 20 × 20 μm. A parallel set of phase images (2 × 2 μm, Nanoscope V, PIR contrast) is shown in Figure S2. Considering the 14–16 wt% FSN nanoparticles, comparable near-surface morphologies might be expected but are not observed. From the phase images in Figs. 1 and 2 and S1, and S2, a range of near-surface morphologies is observed with increasing siliceous domain content. When PDES content is low, the near-surface concentration of U-FSN appears low. The surface morphology for the 4X composition is dominated by the amorphous PDMS volume fraction. Near-surface U-FSN are imaged as light features. With increased weight fraction

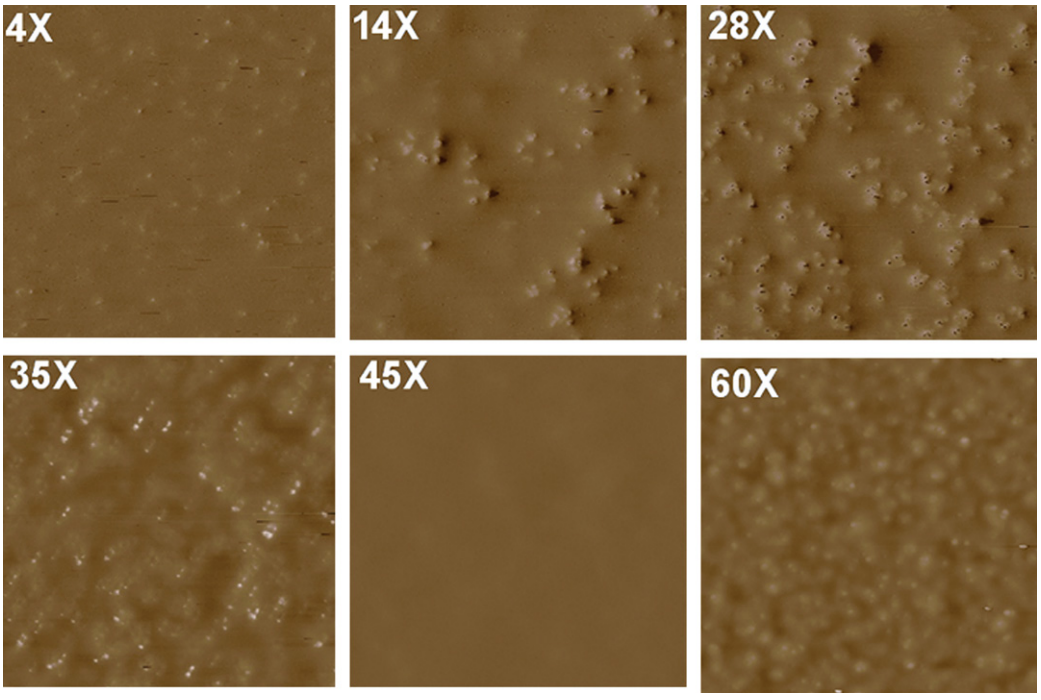

Fig. 2. Phase images (5 × 5 μm, $z = 40°$) for U-FSN nanocomposites (Asylum MFP-3D).

of siliceous domain from 4X to 28X, the apparent concentration of near-surface nanoparticles increases. These higher resolution images confirm that increasing the siliceous phase content to 35X results in an apparent diminution of near-surface nanoparticle concentration. At 45X near-surface nanoparticles are not imaged or "disappear". At 60X, the near-surface nanoparticles "reappear" with larger apparent size, moderate contrast, and high near-surface concentration. An enlarged phase image (20 × 20 μm) for U-FSN-60X is shown in Figure S3. The high density of near-surface nanoparticles and more clearly defined appearance are noteworthy.

3.3. PDMS/U-FSN surface topology

AFM height images (2D, 3D, 20 × 20 μm) for U-FSN nanocomposites are shown in Fig. 3. The RMS roughness, R_q, is shown as a function of composition in Fig. 4. RMS roughness increases from 28 nm to a maximum of 62 nm at 28X followed by a steep decline to 8 nm at 45X; a slight increase to 13 nm is found for 60X. As is usually found, RMS roughness depends on the scan size. The noteworthy coincidence of the minimum in R_q and the "disappearance" of near-surface U-FSN (Figs. 1 and 2, S1, S2) was an important consideration in the development of the proposed model for near-surface morphology.

3.4. PDMS/T-FSN surface morphology and topology

Coatings were prepared by the process described in Scheme 1 using *trimethylsilylated* fumed silica nanoparticles (T-FSN). Figure S5 shows TM-AFM 2D height, phase and 3D height images (20 × 20 μm) for 4-, 28- and 60X T-FSN nanocomposites; from Figure S5, R_q is 7.5, 7.1, and 7.7 nm, respectively. In the case of T-FSN, the near-surface morphology and topology for the processing method described in Scheme 1 are identical to that observed previously for hand mixing. That is, the images are virtually devoid of near-surface features, nanoparticles are not detected/imaged or appear very faintly, and surfaces have very low RMS roughness. Thus, the processing dependence of morphology and topology for U-FSN nanocomposites on the siliceous domain content must stem from chemical interactions of PDMS, PDES, and U-FSN.

3.5. PDMS/FSN fracture surface morphology and topology

TM-AFM images for all U-FSN fracture surfaces are shown in Figures S6 and S7. Height (2D, 3D) and phase images have a similar appearance for all compositions, but there is a noticeable trend to somewhat higher content of areas imaged as "hard". This is expected based on increase of siliceous domain content from <1 to ~13 wt% (Table 1).

A representative set of images for a 45X fracture surface is shown in Fig. 5. The clear nanoparticle imaging in Fig. 5 contrasts with the "disappearance" of nanoparticles for this composition shown in Figs. 1 and 2, S1, and S2. Like all fracture surfaces shown in Figures S6 and S7, R_q for 45X is high, whereas R_q for the 45X coating surface is less than 10 nm.

3.6. Surface wetting characteristic

When possible, we have reported dynamic contact angle (DCA) data for silicones and related coatings [48,49]. However, the PDMS/nanocomposite resins were too viscous for two-sided dip coated samples. Only static contact angle measurements could be obtained for the spin coated films. Static contact angles are shown as

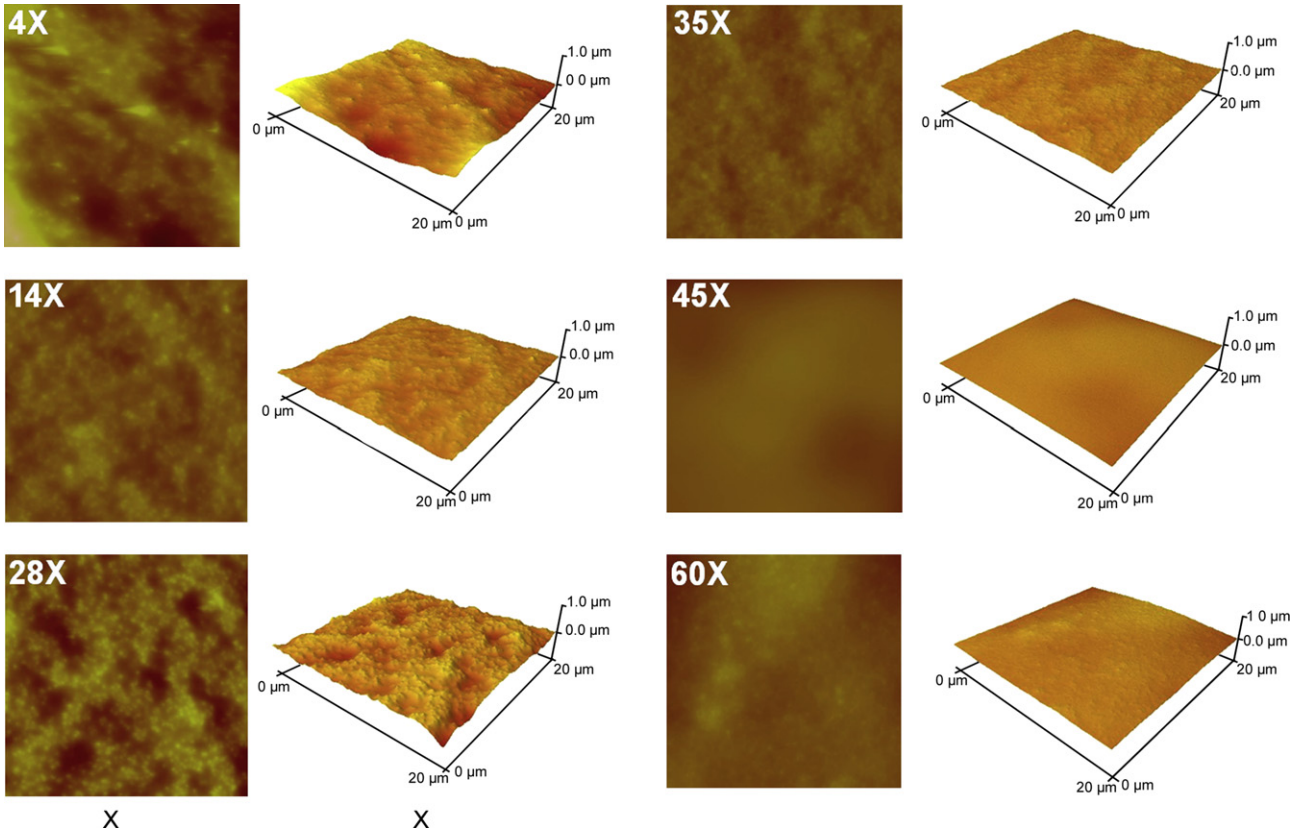

Fig. 3. TM-AFM 2D (left) and the 3D (right) height images (20 × 20 μm) for U-FSN nanocomposites; R_q values are in Fig. 4 (Nanoscope V).

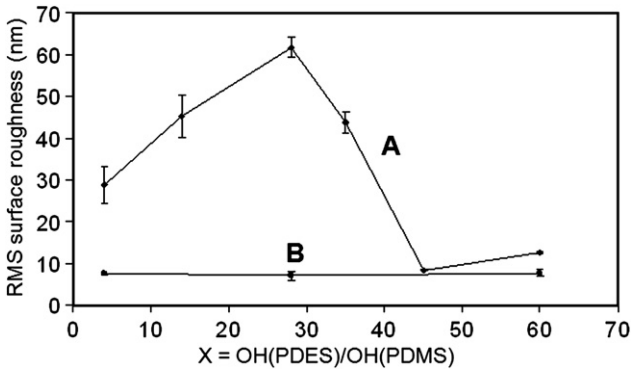

Fig. 4. Variation in the RMS surface roughness (R_q) for 20 × 20 μm 2D height images: **A**, U-FSN; **B**, T-FSN nanocomposites.

a function of PDES(OEt)/PDMS(OH)$_2$ ratio (X) in Fig. 6. A regular decrease in contact angles occurs with increasing siliceous phase content. The highest contact angle is for 4X (115°) while the lowest (100°) is for 60X.

4. Discussion

The intent of changing processing conditions for the PDMS nanocomposites was simply to achieve more homogenous nanoparticle dispersion. Surprisingly, the near-surface nanoparticles "report" that high speed mixing changes AFM imaged near-surface morphology (Figs. 1 and 2, S1, S2). The interpretation of the "message" reported by near-surface nanoparticles must take into account:

i. T-FSN nanocomposites
a. Images are virtually devoid of near-surface features; that is, nanoparticles are not detected/imaged or appear very faintly (Figure S5); T-FSN nanoparticles do not "report" as the trimethylsilylated are chemically inert.
b. Surfaces have uniformly low RMS roughness
c. Near-surface morphology and topology for the processing method described in Scheme 1 is identical to that observed previously for hand mixing.
ii. U-FSN nanocomposites
d. Roughness (R_q) is strongly dependent on siliceous domain wt % (Fig. 4).
e. Compared to hand mixing where nanoparticles "disappeared" at 14X, the same phenomenon occurred at 45X when high speed mixing was employed.
iii. Considerations common to T-FSN and U-FSN
f. Due to condensation cure a steady increase in shrinkage occurs with increased initial PDES content (Table 1); shrinkage reaches 12.3 vol% for 60X.
g. AFM bulk fracture surface images for T-FSN and U-FSN are virtually indistinguishable.

The model proposed in Fig. 7 is an integration of prior results for VLS mixing technique (Fig. 7A), new results for HS mixing (Fig. 7B) and T-FSN PDMS nanocomposites (Fig. 7C). The model for "disappearing" and reappearing nanoparticles described earlier is unchanged (Fig. 7A). That is, at 14X, the surface siliceous domain blocks detection of the U-FSN. At higher siliceous domain volume fractions, the ready reaction of PDES ethoxy and hydroxy groups (Si—OEt$_{PDES}$, Si—OH$_{PDES}$) with U-FSN surface Si—OH (Si—OH$_{nano}$) effects a mechanical connection of the AFM tip with the nanoparticles, which are easily imaged. T-FSNs are inert and are not detected or provide very faint images (Fig. 7C).

The model for U-FSN PDMS nanocomposites generated by HS mixing (Fig. 7B) is based on competition of reactive PDMS end groups (Si—OH$_{PDMS}$) and PDES ethoxy and hydroxy groups (Si—OEt$_{PDES}$, Si—OH$_{PDES}$) for U-FSN surface Si—OH (Si—OH$_{nano}$).

Stage 1. With reference to Scheme 1, initial HS mixing of PDMS and U-FSN (2700 rpm; 4 × 60 s) results in PDMS chain ends bound to U-FSN nanoparticles. At this stage, the interaction may be through H-bonding (chemisorption) or covalent bonding (condensation to Si—O—Si). Scheme 1 (upper right) represents bonded chains with bold lines and nanoparticles to which these chains are bound as filled circles. Fig. 7B depicts four PDMS chains as small circles attached to nanoparticles. The depiction ignores the broad molecular weight distribution of PDMS chains and the disparity between the size of U-FSN (~ 50 nm) and 26 kDa PDMS chains. For the latter, the RMS end-to-end distance is ~7.5 nm using the valence angle model [50].

Stage 2. After addition of PDES, competition for reaction of Si—OH$_{PDMS}$, Si—OEt$_{PDES}$, and Si—OH$_{PDES}$ with Si—OH$_{nano}$ occurs. A myriad of condensation reactions are simultaneously underway as network formation that parallels sol—gel chemistry is initiated. PDES is comprised of multiple species including dimers, trimers, tetramers, and oligomeric species [35] all of which can undergo condensation reactions with PDMS chain ends, other PDES species, and Si—OH$_{nano}$. However, the presence of adsorbed or chemisorbed PDMS chains on U-FSN blocks reaction of PDES species with Si—OH$_{nano}$.

The model in Fig. 7B is based on the notion that nanoparticle-bound PDMS chains form a kinetic barrier to reaction of PDES species with Si—OH$_{nano}$. A corollary to this proposed scheme is that nanoparticles with bound PDMS chains tend to have higher near-surface concentrations compared to U-FSN. Such nanoparticles with bound PDMS chains may be designated "S-FSN". The suggestion that S-FSN tend to have higher near-surface concentrations

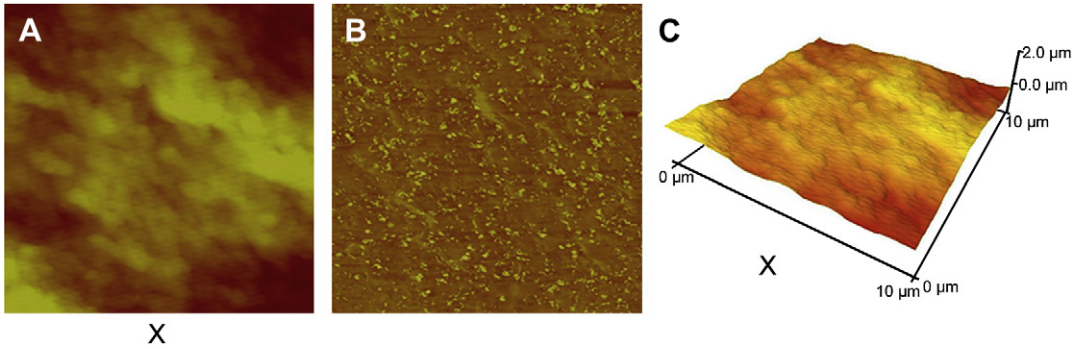

Fig. 5. Representative 20 × 20 μm AFM fracture surface images for U-PDMS-45X: **A**, 2D height; **B**, phase; and **C**, 3D height. The orientation of the x axis in the 3D height image is shown.

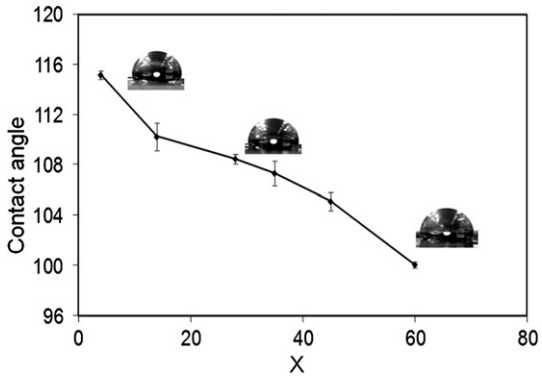

Fig. 6. Static contact angles of the coated slides with variation in the siliceous phase concentration.

compared to U-FSN follows their lower surface free energy and better compatibility with the PDMS matrix.

It follows from the model proposed in Fig. 7B that the near-surface concentration of S-FSN shifts the "disappearance" of nanoparticles to higher siliceous domain concentration (45X-) compared to compositions prepared by very low speed (VLS) processing conditions where U-FSN are the dominant nanoparticle species (Fig. 7A). "Disappearance" is a gradual process as AFM phase images of 35X show the beginning (Figs. 1 and 2, S1, S2). The "reappearance" of nanoparticles at 60X results from a higher concentration of PDES overcoming the blocking effect of surface concentrated PDMS chains. That is, increased PDES results in increased concentration of numerous molecular intermediates containing –Si–OH that compete for the formation of –Si–O–Si– bonds on the nanoparticle surfaces. In turn, this results in enhanced mechanical connectivity to the AFM probe by virtue of the increased near-surface volume fraction of rigid siliceous phase depicted in the last frame of Fig. 7B.

The proposed emergence of the siliceous domain at high PDES concentration (45X) seems counter-thermodynamic. Based on self-condensation alone, the PDES-derived siliceous domain should be polar and glass-like precluding surface concentration. Nevertheless, contact angles decrease regularly (decreasing hydrophobicity) from the lowest (5X, 114°) to highest (60X, 100°) siliceous content (Fig. 6). From wetting behavior, we conclude that the siliceous domain has a gradually increasing, water accessible area fraction, decreasing the water contact angle by 14° at 60X. This emergence is likely facilitated by increased volumetric shrinkage at higher siliceous domain content, as this phase is relatively rigid and less mobile compared to the PDMS-rich domain.

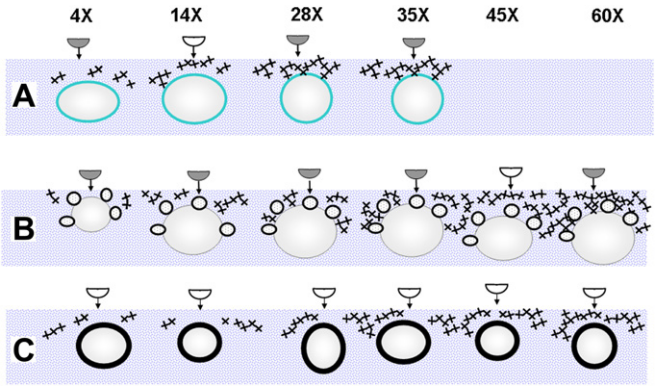

Fig. 7. Model for surface morphology of U-FSN/PDMS nanocomposites as a function of siliceous domain content: **A**, hand mixed; **B**, high speed mixing; **C**, T-FSN nanocomposite. AFM tip indicates nanoparticle imaged (green) or not (red); "**x**" represents siliceous domain Si(–O–)4 tetrahedron; background pattern is PDMS matrix. For interpretation of the references to colour in this figure legend, the reader is referred to the web version of this article.

The combined reaction of PDMS and PDES with the nanoparticles apparently results in nanoparticle aggregates due to PDMS chain/siliceous domain bridging. Aggregates result in increased roughness (R_q, Fig. 4) that is synergistic with increased shrinkage until the 45X composition, where the formation of a continuous near-surface siliceous domain results in a precipitous drop in R_q and nanoparticle "disappearance". The "reappearance" at 60X must result from the connection of the smooth, surface siliceous-rich domain with near-surface nanoparticles via bridging. Such bridges are rigid and afford a mechanical connection of the tip to the near-surface nanoparticles.

5. Conclusion

U-FSN/PDMS nanocomposites prepared using high speed (HS) mixing has a compositional dependent surface morphology (Figs. 1 and 2) which is different from that obtained previously for identical compositions using a VLS mixing technique. A surface morphological model (Fig. 7B) is proposed based on a competition for U-FSN surface Si–OH ($Si–OH_{nano}$) by PDMS –Si–OH end groups ($Si–OH_{PDMS}$) and PDES ethoxy and hydroxy groups ($Si–OEt_{PDES}$, $Si–OH_{PDES}$). At low PDES concentrations (4X–35X), nanoparticle-bound PDMS (S-FSN) inhibits reaction of PDES species with $Si–OH_{nano}$. In addition, nanoparticle-bound PDMS chains facilitate matrix compatibility and near-surface concentration as well as surface roughness accompanying shrinkage. At 45X, the growing concentration of siliceous domain results in a continuous near-surface siliceous-rich domain and nanoparticle "disappearance" (Fig. 1, S1, and 7B, 45X). A noteworthy reduction in coating roughness accompanies the formation of this continuous surface layer (Fig. 4). This is the same phenomenon proposed previously for the 14X composition processed by VLS mixing (Fig. 7A 14X). [37,38] However, the mild processing conditions utilized previously must not have facilitated the "mechano-chemistry" that occurs under HS mixing, viz., the reaction of PDMS –OH chain ends with $Si–OH_{nano}$. Under mild VLS "hand mixing" used previously, PDES competed more favorably for $Si–OH_{nano}$ resulting in nanoparticle "disappearance" at a lower siliceous domain content (14X).

At the 60X composition, nanoparticles "reappear". This detection is attributed to a mechanical connection through the near-surface siliceous domain that enables tip–nanoparticle interactions (Fig. 1, S1, and 7B, 60X). The reduced contrast of the nanoparticles in the 60X phase image (Fig. 1B) is attributed to reduced tip–nanoparticle interactions due to the intervening siliceous domain.

While the emergence of a polar siliceous domain surface area fraction seems counter-thermodynamic for coatings generated in air, water contact angles decrease by 14° from 4X to 60X compositions; that is, the PDMS nanocomposites become less hydrophobic at high siliceous domain content (Fig. 6). Volumetric shrinkage (loss of ethanol) accompanies higher initial polydiethoxysiloxane weight fractions, which may result in increased surface exposure of siliceous domain. The presence of PDMS chains bound to the near-surface siliceous domain presumably acts to buffer against an even steeper decline in water contact angles.

The results reported herein are guiding additional studies aimed at understanding the complex interplay of composition and processing that affect the morphology for systems containing PDMS, nanoparticles, and a siliceous domain from condensation cure. The goal is to obtain additional insights that will facilitate systematic tuning of properties for these important materials, which are used widely in applications ranging from caulks, sealants, and foul-release marine coatings to sophisticated biomaterials.

Acknowledgement

KJW thanks the National Science Foundation (DMR – grants DMR-0207560 and DMR-0802452) and the Office of Naval Research (Contract N00014-08-1-0922) for support of this research.

Appendix. Supplementary data

Supplementary data associated with this article can be found, in the online version, at doi:10.1016/j.polymer.2010.09.053.

References

[1] Ogoshi T, Itoh H, Kim KM, Chujo Y. Macromolecules 2002;35(2):334–8.
[2] Gilman JW, Kashiwagi T, Lichtenhan JD. Sampe Journal 1997;33(4):40–6.
[3] Cudzilo S, Kicinski W. Propellants Explosives Pyrotechnics 2009;34(2):155–60.
[4] Novak BM. Advanced Materials 1993;5(6):422–33.
[5] Sumfleth J, Adroher XC, Schulte K. Journal of Materials Science 2009;44 (12):3241–7.
[6] Ogoshi T, Chujo Y. Macromolecules 2003;36(3):654–60.
[7] Donaldson K, Aitken R, Tran L, Stone V, Duffin R, Forrest G, et al. Toxicological Sciences 2006;92(1):5–22.
[8] Holder E, Tessler N, Rogach AL. Journal of Materials Chemistry 2008;18 (10):1064–78.
[9] Mao YB, Park TJ, Wong SS. Chemical Communications 2005;46:5721–35.
[10] Kojima Y, Usuki A, Kawasumi M, Okada A, Fukushima Y, Kurauchi T, et al. Journal of Materials Research 1993;8(5):1185–9.
[11] Giannelis EP, Krishnamoorti R, Manias E. Polymer-silicate nanocomposites: model systems for confined polymers and polymer brushes. Polymers in Confined Environments 1999;vol. 138:107–47.
[12] Giannelis EP, Zhu J, Park B, Seo KH. Composite of high melting polymer and nanoclay with enhanced properties. Application: US: (USA). 2005. p. 4.
[13] Lu JX, Wong CP. IEEE Transactions on Dielectrics and Electrical Insulation 2008;15(5):1322–8.
[14] Ravirajan P, Peiro AM, Nazeeruddin MK, Graetzel M, Bradley DDC, Durrant JR, et al. Journal of Physical Chemistry B 2006;110(15):7635–9.
[15] Bokobza L. Reinforcement of elastomeric networks by fillers. Wiley-V C H Verlag GmbH; 2001. pp. 243–260.
[16] Bokobza L, Rapoport O. Journal of Applied Polymer Science 2002;85 (11):2301–16.
[17] Clarson SJ, Semylen JA, editors. Siloxane polymers. New Jersey: Prentice Hall; 1993. p. 560.
[18] Tarno LJ. Deep section cure silicone rubber. U.S. Dow Corning Corp.; 1968.
[19] Burnside SD, Giannelis EP. Chemistry of Materials 1995;7(9):1597–600.
[20] Garrido L, Mark JE, Sun CC, Ackerman JL, Chang C. Macromolecules 1991;24 (14):4067–72.
[21] Stevenson I, David L, Gauthier C, Arambourg L, Davenas J, Vigier G. Polymer 2001;42(22):9287–92.
[22] Winberg P, Eldrup M, Maurer FHJ. Polymer 2004;45(24):8253–64.
[23] Wen J, Mark JE. Journal of Materials Science 1994;29(2):499–503.
[24] Mark JE. Current Opinion in Solid State & Materials Science 1999;4 (6):565–70.
[25] Sun CC, Mark JE. Polymer 1989;30(1):104–6.
[26] Warrick EL, Pierce OR, Polmanteer KE, Saam JC. Rubber Chemistry and Technology 1979;52(3):437–525.
[27] Okamoto T, Nakamura S. Thermal endurance, electrical insulating, and mechanical properties of hybrid made with poly(dimethylsiloxane) and tetraethoxysilane. Institute of Pure and Applied Physics; 2008:521–6.
[28] Hillborg H, Gedde UW. IEEE Transactions on Dielectrics and Electrical Insulation 1999;6(5):703–17.
[29] Unger MA, Chou HP, Thorsen T, Scherer A, Quake SR. Science 2000;288 (5463):113–6.
[30] Botter W, Soares RF, Galembeck F. Journal of Adhesion Science and Technology 1992;6(7):791–805.
[31] Prasad BR, Brook MA, Smith T, Zhao S, Chen Y, Sheardown H, et al. Colloids and Surfaces B-Biointerfaces;78(2):237–242.
[32] Johann RM, Baiotto C, Renaud P. Biomedical Microdevices 2007;9(4):475–85.
[33] Bullock S, Johnston EE, Willson T, Gatenholm P, Wynne KJ. Journal of Colloid and Interface Science 1999;210(1):18–36.
[34] Berglin M, Wynne KJ, Gatenholm P. Journal of Colloid and Interface Science 2003;257(2):383–91.
[35] Cihlar J. Colloids and Surfaces A-Physicochemical and Engineering Aspects 1993;70(3):253–68.
[36] Wynne KJ, Ho T, Johnston EE, Myers SA. Applied Organometallic Chemistry 1998;12(10–11):763–70.
[37] Inagi S, Ogoshi T, Miyake J, Bertolucci M, Fujiwara T, Galli G, et al. Chemistry of Materials 2007;19(9):2141–3.
[38] Ogoshi T, Fujiwara T, Bertolucci M, Galli G, Chiellini E, Chujo Y, et al. Journal of the American Chemical Society 2004;126(39):12284–5.
[39] Magonov SN, Elings V, Whangbo MH. Surface Science 1997;375 (2–3):L385–91.
[40] Johnston E, Bullock S, Uilk J, Gatenholm P, Wynne KJ. Macromolecules 1999;32(24):8173–82.
[41] Garrett JT, Siedlecki CA, Runt J. Macromolecules 2001;34(20):7066–70.
[42] Makal U, Fujiwara T, Cooke RS, Wynne KJ. Langmuir 2005;21(23): 10749–55.
[43] Agnihotri A, Garrett JT, Runt J, Siedlecki CA. Journal of Biomaterials Science-Polymer Edition 2006;17(1–2):227–38.
[44] Kurt P, Wood L, Ohman DE, Wynne KJ. Langmuir 2007;23:4719–23.
[45] Garcia R, San Paulo A. Physical Review B 1999;60(7):4961–7.
[46] Stark RW, Schitter G, Stemmer A. Physical Review B 2003;68(8).
[47] Round AN, Miles MJ. Nanotechnology 2004;15(4):S176–83.
[48] Uilk JM, Mera AE, Fox RB, Wynne KJ. Macromolecules 2003;36(10):3689–94.
[49] Zhang W, Zheng Y, Orsini L, Morelli A, Galli G, Chiellini E, et al. Langmuir;26 (8):5848–5855.
[50] Chanda M. Advanced polymer chemistry. New York: Marcel Dekker; 2000.